

1

Introduction to Upconversion and Upconverting Nanoparticles

Manisha Mondal^{1,2} and Vineet Kumar Rai¹

¹Indian Institute of Technology (Indian School of Mines), Department of Physics, Laser and Spectroscopy Laboratory, Dhanbad 826004, Jharkhand, India

²Tezpur University (Central University), Department of Physics, Napaam, Tezpur, Sonitpur 784028, Assam, India

1.1 Introduction

Spectroscopy almost deals with the interaction of light and matter. It provides information about splitting of electromagnetic radiation into its constituent wavelengths. The beginning of spectroscopy lies since the observation of light dispersion through prism by Sir Isaac Newton. Among different spectroscopy techniques, optical spectroscopy delivers an exceptional tool by which one can find detailed information regarding the absorbing and emitting atoms, ions, molecules, defects, their local surroundings, etc. In a term, optical spectroscopy allows light to penetrate inside materials. Optical spectroscopy can be characterized into four parts: absorption, luminescence, reflection, and scattering. A marvelous dimension of research carried out in finding novel luminescent materials plays an important role in optical communication, lighting, medical diagnosis, etc. (Berthou and Jörgensen 1990; Cheng et al. 2013; Jiang et al. 2016; Lin et al. 2016; You et al. 2016; Dey and Rai 2017; Mehra et al. 2020). When an atomic system after absorbing the photons of appropriate frequency transits upward to a higher state and then by the spontaneous emission process, it may return to the ground state. This de-excitation route is familiar as the luminescence process. The occurrence of luminescence due to excitation of light is known as photoluminescence. On the other hand, luminescence due to excitation of an electron beam is termed as cathodoluminescence, which helps to identify impurities, lattice defects, and crystal distortions. Radioluminescence occurs due to excitation through the highly energetic electromagnetic radiations (i.e. α rays, β rays, and γ rays). The thermoluminescence phenomena are used in radiation dosimetry, dating of minerals and old ceramics, materials characterization, biology, forensic, etc. It occurs when a material radiates light as a consequence of release of energy kept in traps by thermal heating. Electroluminescence occurs due to the passage of electric current over a material. The emission of light due to mechanical disturbance originates triboluminescence. Conferring to the diverse positions of

the excitation and emission bands, the luminescent materials can be categorized into Stokes- and anti-Stokes-type luminescent materials. These processes are typically exemplified by the Jablonski diagram (Jablonski 1935; Jablonski 1993). The luminescent materials are commonly known as phosphors, which means “light bearer,” that consist of host and dopants. In these constituents, lanthanide materials are mainly introduced into the host matrix. Lanthanides have the most complicated electronic structures because of their large number of incomplete 4f energy levels. The present chapter presents a brief outlook on understanding the frequency conversion mechanisms, electronic energy levels of rare-earth (RE) ions, transition metal ions, theoretical description of the optical characteristics of RE ions, and Upconverting nanoparticles (UCNPs).

1.2 Frequency Conversion and Its Various Processes

The photoluminescent materials are able to display visible emissions via suitable ultraviolet (UV) or near-infrared (NIR) excitations. In the majority of cases, excitation energy is greater than emitted photon energy; this emission is called as Stokes emission, and the corresponding energy loss is known as Stokes shift. In certain circumstances, emitted energy is higher than absorbed energy; this is known as anti-Stokes emission.

1.2.1 Stokes Emission

The Stokes-type emission process possesses two types of features such as downconversion and quantum cutting (Huang et al. 2013; Loo et al. 2019). In quantum cutting process, two or more lower energy photons are emitted for each incident high-energy photon absorption. In this process, two, three or four low-energy photons are emitted because of the absorption of one NIR, visible, or ultraviolet photon. In this process, the conversion efficiency is more than 100%. In current years, quantum cutting has acknowledged considerable devotion as a budding method to improve the photovoltaic conversion efficiency of solar cells. On the other hand, in the downconversion process, emission of one lower energy photon takes place because of the absorption of one higher energy photon; thus, the conversion efficiency will not go beyond 100%.

1.2.2 Anti-Stokes Emission

The anti-Stokes emission process occur via three processes: two-photon absorption (TPA), second harmonic generation (SHG), and upconversion (UC) (Figure 1.1) (Pollnau et al. 2000; Gamelin and Gudel 2000; Suijver 2008; Grzybowski and Pietrzak 2013; Chen et al. 2015; Nadort et al. 2016). TPA is a type of nonlinear absorption process that can be defined as the simultaneous absorption of two photons of same or different frequencies by an atom, ion, or molecule. In this process, the electron is promoted from low energy level (i.e. ground state) to excited

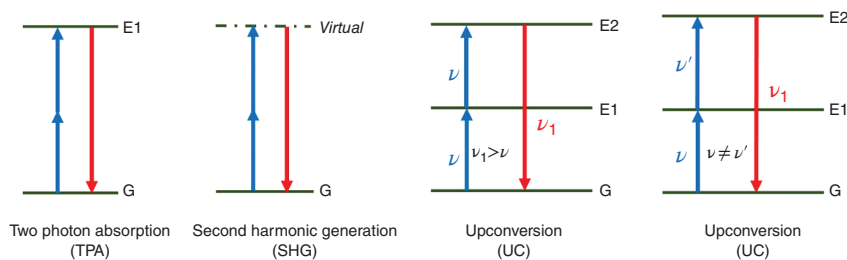


Figure 1.1 Basic energy-level diagrams depicting typical anti-Stokes processes.

level, and the energy of the emission transition is equal to the sum of two-photon energies. As this is a third-order nonlinear process, it is effective at precise high intensities. TPA was initially anticipated by Maria Goeppert-Mayer in the year 1931. This was experimentally verified by the laser after its discovery. A number of techniques are used to measure TPA, such as two-photon excited fluorescence, z-scan, nonlinear transmission, etc. On the other hand, SHG, “an optical nonlinear process,” occurs from a virtual state in a medium having second-order nonlinear susceptibility. This was revealed and experimentally verified by Franken et al. (1961). They detected the second harmonic light when an intense beam of 6943 Å from the ruby laser was passed through the quartz crystal. In this process, two photons of the same frequency interact with a nonlinear material (i.e. medium) and give rise to a new photon of double the frequency or energy of the incident photons. Furthermore, UC is also an anti-Stokes process that converts the lower energy photons into high-energy photons, e.g. infrared to visible or UV light (Figure 1.1). It is a stepwise absorption process involving intermediate states (Auzel 1966; Ovsyakin and Feofilov 1966). Basically, among these three processes of converting lower energy photons into higher energy photons, TPA and SHG need a coherent beam as well as a very high excitation beam intensity. In the UC process, coherent pumping and high intensity of the excitation beam are not necessarily required. It occurs even at low intensity of the excitation beam because of the presence of real intermediate states (generally, of metastable nature).

The materials that exhibit the UC properties are known as upconverting materials. In recent years, these upconverting materials are extensively used in sensing, infrared counters, solid-state lasers, solar cells, fingerprint detection, security ink, upconverters, biological fields, etc. (Digonnet 1993; Wade et al. 2003; Rai 2007; Wang and Liu 2009; Gu et al. 2013; Li et al. 2013; Wang and Zhang 2014; Chen et al. 2014; Mondal and Rai 2020). Generally, the UC phenomenon observed in these materials is not as simple as depicted in Figure 1.1. Several processes accountable for UC mechanisms are as follows.

1.2.2.1 Ground/Excited-State Absorption (GSA/ESA)

Ground-state absorption (GSA) is one of the simplest routes for UC mechanism (Auzel 1973, 2004; Garlick 1976; Rai et al. 2013; Reddy et al. 2018). The process in which the ground-state ions (i.e. electrons) after absorbing the requisite energy from the pump photons are promoted to the first intermediate level is known as the GSA

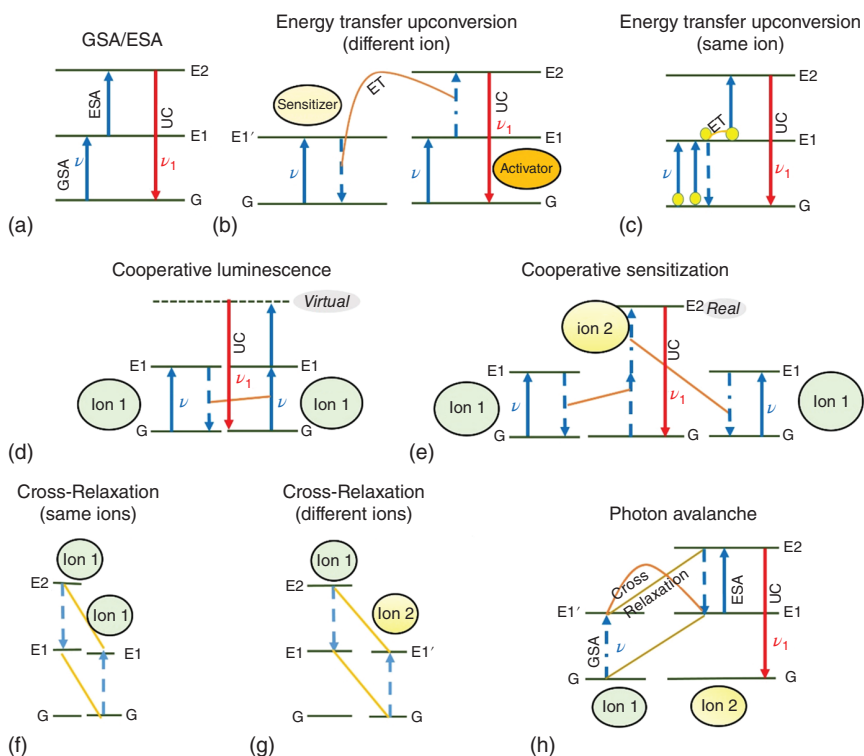


Figure 1.2 Schematic representation of possible UC mechanisms: (a) GSA/ESA, (b and c) ETU, (d) cooperative luminescence, (e) cooperative sensitization, (f and g) CR, and (h) PA processes.

process. Conversely, sequential absorption of two light quanta by a particular ion is known as ESA process (Auzel 1973, 2004; Garlick 1976; Rai et al. 2013). In the case of ESA process, the ion present in the intermediate state absorbs the second photon and transits upward to the next higher state. For example, the energy-level diagrams for GSA and ESA mechanisms are presented in Figure 1.2a. Here at first, an ion absorbs the pump photon of energy ($=h\nu$, where “ h ” is Planck’s constant and “ ν ” is the frequency of the incident photon) and reaches to the intermediate state E1 (exhibit long lifetime) from the ground state G via the GSA process and then a second pump photon (of the same energy) excites the ion from E1 state to the next higher state E2. A radiative decay of the ion from the excited state (E2) to the ground state (G) results in UC emission. Thus, a single ion is involved in the whole ESA process. For getting proficient UC emission through the ESA process, a ladder-like energy-level arrangement in ions is essential.

1.2.2.2 Energy Transfer Upconversion (ETU)

Like the ESA process, the energy transfer upconversion (ETU) process also involves successive absorption of two energy quanta by the ions to occupy the intermediate (i.e. metastable) state (Figure 1.2). As in the ESA process there is an involvement

of single ion, however, ETU operates within two (similar or different) ions. In this mechanism, the involved two dopant ions are termed as sensitizer and activator (Heer et al. 2003; Boyer et al. 2007; Shan et al. 2007; Soni et al. 2015; Mukhopadhyay and Rai 2020; Pattnaik and Rai 2020). At first, both the (different) ions absorb the pump photons from the ground state and then moves to their respective metastable states ($E1'$ and $E1$, where $E1' \cong E1$) through the GSA process (Figure 1.2b). After that, the sensitizer ion (present in $E1'$ state) handovers its excitation energy to the neighboring activator ion (present in $E1$ state) and relaxes back to the ground state. The activator ion after gaining this excitation energy from the sensitizer reaches to the next higher energy state ($E2$).

When the two involved dopant ions are similar, these two ions are initially excited to the intermediate state ($E1$) after receiving the energy from pump photons (Figure 1.2c). The two ions present in the $E1$ state exchange their energy in such a way that one ion (i.e. donor), after transferring its excitation energy to the other excited ion (i.e. acceptor), decays nonradiatively to the lower energy level (G). The other ion (i.e. acceptor) after getting excitation energy from the first one (i.e. donor) is promoted to the next higher energy state ($E2$). A radiative transition from state $E2$ to the ground state (G) generates a photon of energy ($=h\nu_1$), which is higher than the incident photon energy ($=h\nu$) (Figure 1.2). This ETU process is the most efficient UC emission process (Auzel 2004; Rai et al. 2007, 2008). In this process, the dopant ion concentration (which regulates the average distance concerning adjacent dopant ions) plays a key role in the UC emission intensity.

1.2.2.3 Cooperative Luminescence and Cooperative Sensitization Upconversion (CSU)

UC emission by a cooperative energy transfer process involves two ions (one acts as a donor and the other ion as an acceptor). In the cooperative luminescence process, two ions absorb the pump photons successively and reach the higher (intermediate) state $E1$ (Figure 1.2d). In this intermediate level, these two ions transfer their energy in such a way that one ion (donor) transfers its excitation energy to the other one (acceptor) and the donor returns to the ground state (G). The acceptor, after gaining the excitation energy from the donor, transits upward to a higher energy state, “which is a virtual state.” This virtual state is also known as the cooperative energy state (Lee et al. 1984; Maciel et al. 2000; Diaz-Torres et al. 2005). From this virtual state, it relaxes radiatively to the ground state (G) via emitting a photon of energy larger than the incident photon energy (Figure 1.2d). On the other hand, in the cooperative sensitization process, when the energy of the two excited ions are transferred to a third ion (ion 2), then it goes from the ground state to an excited state having energy equal to the sum of the energies of the two individual ions (Martín et al. 2001; Salley et al. 2001, 2003). In Figure 1.2e, the excitation energy of the two excited ions (ion 1) present in the state $E1$ is transferred to a third ion (ion 2). The third ion (ion 2) present in the ground state (G), after absorbing the excitation energy corresponding to the two excited ions (ion 1), moves to its higher state ($E2$). After that, the third ion from the excited state ($E2$) relaxes radiatively to the lower levels (say ground state) via emitting the photons of energy higher than that of

the incident photon. This process is known as cooperative sensitization, and the emitting state (E2) in this process is a real state (Figure 1.2e). Thus, the cooperative sensitization is more effective than cooperative luminescence because it may compensate the low UC emission efficiency (Dwivedi et al. 2007; Liang et al. 2009).

1.2.2.4 Cross-relaxation (CR) and Photon Avalanche (PA)

The cross-relaxation (CR) process occurs due to ion–ion interaction (ions may be similar or different) (Chen et al. 2014; Pattnaik and Rai 2020) (Figure 1.2f,g). The cross-relaxation between two identical ions/molecules is responsible for self-quenching (Figure 1.2f). In the self-quenching process, the intermediate states of both the ions (ion 1) have the same energy (E1). When the cross-relaxation occurs between two different ions (Figure 1.2g), the first ion shares a part of its excitation energy to the second ion by the process $E2(\text{ion } 1) + G(\text{ion } 2) \rightarrow E1(\text{ion } 1) + E1'(\text{ion } 2)$ (Figure 1.2g). In this process, the first ion (ion 1) initially present in the excited state (E2) interchanges a part of its excitation energy to the second ion (ion 2) that is initially available in the ground state (G). By this way, the decrease in the energy of the first ion (ion 1) is equal to the increase in the energy of the second ion. This results in both the ions/molecules changing simultaneously to the excited state (E1 and E1'). Among the other UC processes, the most exciting process is photon avalanche (PA), which was first experimentally observed in Pr³⁺-doped infrared quantum counters (Chivian et al. 1979). Generally, this PA process occurs when the excitation energy exceeds its threshold limit. When the excitation energy is lower than the threshold energy, the emitted intensity is very poor, but as it exceeds the limit, the emitted intensity becomes enormously greater (Joubert 1999; Singh et al. 2011; Zhu et al. 2012; Mondal et al. 2016). For occurrence of PA process, at first, the intermediate level and the upper excited level are populated by the GSA, ESA, and ETU processes. By the CR process between these upper excited level and the ground state of a neighboring ion, two ions are generated in the intermediate level E1 (Figure 1.2h). Now, two ions are available in the intermediate state for the ESA process. Thus, with the feedback looping of ESA and CR processes simultaneously, the number of ions in the intermediate level increases, which give rise to strong UC emission.

The PA process is an unusual pumping process because it may lead to strong UC emission from the upper excited state E2 without any resonant GSA from the ground state (G) to the intermediate state (E1) of ion 2 (Figure 1.2h). The frequency of incident photon is in resonant with state E1' of ion 1 and the upper excited state E2 of ion 2. An efficient CR process, i.e. $E2(\text{ion } 2) + G(\text{ion } 1) \rightarrow E1(\text{ion } 2) + E1(\text{ion } 1)$, occurs between ion 1 and ion 2. This results in both the ions to occupy the intermediate state E1. These two ions readily populate the level E2 through ESA to further initiate the cross-relaxation. With the feedback looping of these efficient cross-relaxation and ESA processes, the number of ions in the intermediate state E1 increases rapidly, which results further an enormous increase in the population of level E2. Thus, in the PA process, a strong UC emission from state E2 to the ground state G (of ion 2) has been observed.

1.3 Transition Metals and Their Properties

The optical centers are necessary for the perfect crystals to exhibit the optical spectra. Depending on the absorption and emission bands of the optical centers present in the pure crystals, they are pertinent for diverse applications, such as optical amplifiers, solid-state lasers, color displays, absorbers, improving in luminescence brightness, fibers, optical switches, etc. Any element in the periodic table may act as a foreign element in the crystal. However, essentially, a few number of elements can be ionized, which can generate energy levels and thus yield optical features. For industrial applications, the two extremely important elements are transition metals and REs in the periodic table. Transition metal ions are especially used as optically active dopants in tunable solid-state lasers (Solé et al. 2005). These ions belong to the fourth period of the periodic table with electronic configuration $1s^2 2s^2 2p^6 3s^2 3p^6 3d^n$, where “ n (varies from 1 to 10)” is the number of 3d electrons present in the transition metal ions. Generally, valence electrons are responsible for optical transitions; hence, in the case of transition metals, 3d electrons are accountable. Because of the large radius of transition metal ions as compared to lanthanides and no shielding of valence electrons, strong field effect occurs; hence, they exhibit the broad bands.

The Sugano–Tanabe diagram explains the energy-level diagram for the transition metal ions (Figure 1.3) (Tanabe and Sugano 1954a,b). The spectroscopic terms for the free ion states of the transition metal ions due to the L-S interaction are described

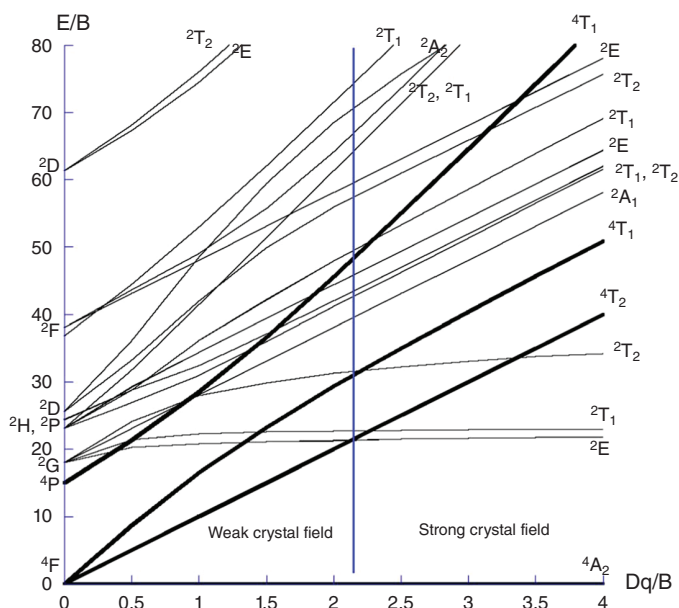


Figure 1.3 Tanabe–Sugano diagram for the d^5 electron configuration in the octahedral crystal field. Source: Brik et al. (2016). Reprinted with permission of The Electrochemical Society.

as $^{2S+1}L_J$, where, L , S , and J denote the total orbital angular momentum, total spin angular momentum, and total angular momentum, respectively. The energy separation among the ^{2S+1}L states, i.e. the strength of the electron–electron interaction, can be calculated with the help of Racah parameters (A, B, and C) (Solé et al. 2005). On the basis of octahedral crystal lattice, Sugano and Tanabe explained the occurrence of energy levels in the case of transition metal ions, but by using this diagram, one can also interpret the optical spectra arising from the transition metal ions in different types of host lattices.

This diagram explains the splitting of ^{2S+1}L free ion energy states with the ratio between the strength of the crystal field and the electron–electron interaction strength (symbolized as Dq/B) versus the free ion energy levels (E/B units). In this diagram, the y -axis is in terms of energy “ E ” scaled by B (one of the Racah parameters). The splitted terms for ^{2S+1}L energy states are termed as A, T, and E levels. This Sugano–Tanabe diagram also explains the nature of the optical bands for transition metal ions. In the case of strong crystal field approximation, the crystal field effect dominates over the electron–electron interaction among 3d ions. Accordingly, there are three single-electron orbitals for each orbital. Furthermore, according to the Sugano–Tanabe diagram, for low crystal field strength, the emission band is shifted toward the lower energy side. For this specific nature, the emission wavelength in the transition metal ions depends on a particular host material. Thus, doping of transition metal ions in different host materials directed to the advancement of countless varieties of tunable solid-state lasers. Most of the transition metal ions are incorporated in the octahedral crystal host matrix, so their energy level can be explained on the basis of Sugano–Tanabe diagram (Tanabe and Sugano 1956). However, in some cases, such as Ni^{2+} , Co^{2+} , and Cr^{2+} ions, these transition metal ions are incorporated in the tetrahedral crystal lattice for different applications; therefore, the König and Kremer diagram (König and Kremer 1997) is applicable in explaining the energy levels of transition metal ions other than the octahedral one.

1.4 Rare Earths and Their Properties

Most of the lasers, phosphors, amplifiers, etc., comprise RE elements. Surprisingly, the global applications of RE-based materials are increasing from industry applications to medical applications. There are 15 lanthanide elements along with two more elements i.e. scandium (Sc) and yttrium (Y). These 15 lanthanide elements are commonly named as lanthanum (La), cerium (Ce), praseodymium (Pr), neodymium (Nd), promethium (Pm), samarium (Sm), europium (Eu), gadolinium (Gd), terbium (Tb), dysprosium (Dy), holmium (Ho), erbium (Er), thulium (Tm), ytterbium (Yb), and lutetium (Lu). Most of the RE elements are entitled as per the name of the inventors or the name of their revealed places. These RE elements are incorporated in different host materials in their ionized (either divalent or trivalent) form. The divalent RE ions {Eu (+2), Yb (+2), and Sm (+2)} possess one more electron compared to the trivalent ions and thus exhibit different optical features and treat differently.

1.4.1 Trivalent Rare-Earth Ions

The outer most electronic configurations of divalent and trivalent RE ions are $5d 4f^n 5s^2 5p^6$ and $4f^n 5s^2 5p^6$, respectively, where n (varies from $n = 0$ to 14) specifies the number of electrons in the unfilled $4f$ shell. These $4f^n$ electrons are the valence electrons that are accountable for the spectroscopic transitions.

1.4.1.1 Electronic Structure

The presence of valence electrons in the $4f$ shell makes the RE ions as luminescent centers of any phosphor material. The group of 15 elements comprising atomic number starting from 57 to 71 in the sixth period of the periodic table together with scandium (Sc) and yttrium (Y) are known as RE elements. When these RE elements are introduced into the hosts, they easily convert into their either doubly or triply ionized states to acquire their stable electronic configurations. The outer most electronic configurations of lanthanum (La, atomic number $Z = 57$) and the last element lutetium (Lu, $Z = 71$) in their triply ionized state are $4f^0 5s^2 5p^6$ and $4f^{14} 5s^2 5p^6$, respectively. There are fifteen possibilities for filling these $4f$ orbitals as the f orbital contains seven suborbitals. Actually, these unfilled $4f$ valence electrons are in control for optical transitions. Table 1.1 presents the electronic arrangements and ground states of each triply ionized RE element. The actual electronic configuration of the 15 RE elements (i.e. from La to Lu) is $[Xe] 5d^1 6s^2 4f^n$ ($n = 0$ to 14). However, in

Table 1.1 Electronic configuration of trivalent ionic states of RE elements (Shionoya et al. 1998).

Ion	Atomic number	Number of 4f electrons (n) and electronic configuration	$S = \sum s$	$L = \sum l$	$J = L - S$ ($n < 7$) $J = L + S$ ($n \geq 7$)	Ground state
La ³⁺	57	0 and [Xe]4f ⁰	0	0	0	¹ S ₀
Ce ³⁺	58	1 and [Xe]4f ¹	1/2	3	5/2	² F _{5/2}
Pr ³⁺	59	2 and [Xe]4f ²	1	5	4	³ H ₄
Nd ³⁺	60	3 and [Xe]4f ³	3/2	6	9/2	⁴ I _{9/2}
Pm ³⁺	61	4 and [Xe]4f ⁴	2	6	4	⁵ I ₄
Sm ³⁺	62	5 and [Xe]4f ⁵	5/2	5	5/2	⁶ H _{5/2}
Eu ³⁺	63	6 and [Xe]4f ⁶	3	3	0	⁷ F ₀
Gd ³⁺	64	7 and [Xe]4f ⁷	7/2	0	7/2	⁸ S _{7/2}
Tb ³⁺	65	8 and [Xe]4f ⁸	3	3	6	⁷ F ₆
Dy ³⁺	66	9 and [Xe]4f ⁹	5/2	5	15/2	⁶ H _{15/2}
Ho ³⁺	67	10 and [Xe]4f ¹⁰	2	6	8	⁵ I ₈
Er ³⁺	68	11 and [Xe]4f ¹¹	3/2	6	15/2	⁴ I _{15/2}
Tm ³⁺	69	12 and [Xe]4f ¹²	1	5	6	³ H ₆
Yb ³⁺	70	13 and [Xe]4f ¹³	1/2	3	7/2	² F _{7/2}
Lu ³⁺	71	14 and [Xe]4f ¹⁴	0	0	0	¹ S ₀

the triply ionized state, these elements lose their 5d and 6s orbital electrons; hence, the outer most electronic configuration of trivalent RE ions becomes $4f^n 5s^2 5p^6$ (Table 1.1). Therefore, due to the larger radii of 5s and 5p orbitals compared to the 4f orbital, these 4f electrons are shielded by 5s and 5p orbitals. Unlike transition metals when doped into solid materials, the outer 3d electrons are strongly affected by the crystal field effect; in the case of RE ions due to this shielding effect when they are incorporated into a solid host, the 4f electrons are weakly perturbed. Because of this shielding of 4f electrons by the completely filled outer electronic shells ($5s^2 5p^6$), the relative positions of 4f energy levels in the RE ions do not vary very much from one host to the other. Owing to this exceptional property of the triply ionized RE ions, they exhibit sharp absorption and emission spectra and thus have longer lifetime.

1.4.1.2 Interaction of Rare-Earth Ions

The 4f–4f transitions are parity forbidden according to the Laporte selection rule, but when incorporated into a host matrix, the electronic structure of the REs are perturbed, and because of the intermixing of $4f^n$ and $4f^{n-1} 5d$ orbitals, the optical transitions become allowed. Because of this intermixing, the parity of levels is changed and the transitions become allowed. These transitions are known as electric dipole allowed transitions. By using Schrodinger's equation, the energy levels of the RE ions responsible in optical transitions can be calculated as (Auzel 2004; Solé et al. 2005)

$$H\Psi = E\Psi \quad (1.1)$$

where “ Ψ ” is the eigenfunctions of the optical center and “ H ” denotes the Hamiltonian because of the diverse interactions of the 4f orbital electrons. Generally, the crystal field theory and the molecular orbital theory (MOT) have been used to describe the interaction between the RE elements and the host matrices.

Crystal Field Theory The crystal field theory was first described by Hans Bethe and John Hasbrouck van Vleck in the year 1930. In the case of transition metal ions when incorporated in a host material, the outer electrons are greatly affected by the surrounding host environment. However, in the case of RE ions when doped into a host material, the energy levels are only slightly perturbed because of the shielding by the $5s^2 5p^6$ orbitals. This breaking of degeneracy of the d and f electron orbitals can be described on the basis of crystal field theory (Wybourne 1965; Wybourne and Meggers 1965; Carnall et al. 1989; Auzel 2004; Liu 2005, 2015; Solé et al. 2005). The filled orbitals in the case of RE ions are 4d, 5s, and 5p, whereas 4f, 5d, and 6s are valence electron shells in their triply ionized state. Because of the larger radii of 5s and 5p orbitals, the 4f electrons of the RE ions are protected from the surrounding perturbation. The energy levels of the RE elements can be represented by some elementary quantum mechanical terms, total orbital angular momentum L (sum of total quantum number l), total spin angular momentum S (sum of total quantum number s), and the total angular momentum J ($=L + S$). With the help of Schrodinger's equation, the interaction between the RE ions and the host element

can be realized. The overall Hamiltonian (H) of the RE ions subjected to the host surrounding can be defined as

$$H = H_F + H_C \quad (1.2)$$

where H_F is the Hamiltonian of the free ion (i.e. isolated) and H_C is the Hamiltonian arises due to the crystal field, which deals with the interaction between the 4f electrons of the RE ions and the crystal field of the host material.

In the case of isolated, i.e. free RE ions, the Hamiltonian (using the perturbation theory) can be described as

$$H_F = H_0 + H_{ee} + H_{SO} \quad (1.3)$$

where H_0 , termed as the central field Hamiltonian, describes the interaction energy arises in the valence electrons owing to nucleus and electrons of triply ionized REs, H_{ee} describes the interaction energy due to the interaction among valence electrons, and H_{SO} is the spin-orbit interaction energy of the electrons.

The strongest interaction among three interactions is the Coulomb interaction, which signifies the repulsion among 4f valence electrons in the RE ions. The individual orbital angular momentum (l_i) and the spin angular momentum (s_i) of the individual electrons couple each other to form a total orbital angular momentum (L) and total spin angular momentum (S) due to the Coulombic interaction. Because of this interaction, the energy levels of any RE ions are divided into $2S+1L$ folds. The degeneracy of the separated energy levels turn out to be $(2S+1)(2L+1)$ fold, and the energy separation concerning these levels are of the order of $\sim 10^4 \text{ cm}^{-1}$ (Figure 1.4).

The most significant interaction between the host material and the doped RE ions is the spin-orbit interaction. This interaction helps for calculating the free ion multiplet terms. Conferring to the Russell-Saunders scheme, the spin and orbital angular momentum couples with each other, and as a result, the total angular momentum term (J) generates. The value of J varies according to the variation for the filling of orbitals. For less than half-filled $J = L - S$ and for more than

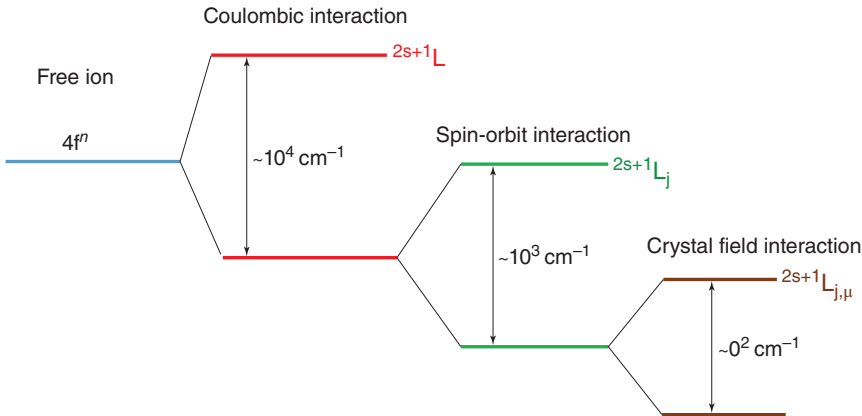


Figure 1.4 Splitting of 4f energy levels under different perturbations (drawn for visualization only).

half-filled shells, the value of $J = L + S$. Because of the spin-orbit interaction, the splitted levels are represented as $^{2S+1}L_J$ levels. In this interaction, the degeneracy of the splitted levels is $(2L + 1)(2S + 1)$ fold, and the order of the separated levels is $\sim 10^3 \text{ cm}^{-1}$ (Figure 1.4). The arrangement of energy levels of these multiplets is decided according to Hund's rule.

The shielding effect of the RE ions causes valence electrons weakly perturbed in the presence of host crystal field. Because of this, the spin-orbit interaction dominates over the crystal field interaction, and this results $(2L + 1)(2S + 1)$ fold degenerate energy levels of the RE ions. Because of this, the optical spectra of the RE ions incorporated into host materials are similar to the free ion spectra. However, while doping the RE ions in host materials, sometimes, a strong crystal field arises (generally because of the more asymmetric nature), and hence, the $^{2S+1}L_J$ levels of the RE ions again show splitting, known as Stark splitting. Degeneracy of Stark splitting depends on the value of electrons present in the outer orbitals. For even values of the 4f electrons, the degeneracy of the $^{2S+1}L_J$ level becomes $(2J + 1)$ fold; however, it becomes $(J + 1/2)$ fold degenerate in the case of odd values of the valence electrons. Therefore, the general representation of the energy level of the dopant ions for Stark splitting is $^{2S+1}L_{J,\mu}$ (μ indicates the numbering of Stark sublevels) and the order of this splitting is $\sim 10^2 \text{ cm}^{-1}$ (Figure 1.4). In the case of transition metal ion-incorporated hosts, the d orbitals are the valence electrons, but they remain unshielded; hence, the crystal field interaction totally changes the energy levels of the transition metals. For example, if the outer arrangement is d^1 , the electron-electron interaction energy term, i.e. H_{ee} , turns out to be zero because of the presence of a single electron in the valence state. Accordingly, in this circumstance, no variance occur between the weak (i.e. H_{SO} governs) and strong crystalline fields (i.e. H_{CF} leads). Then, again for d^n configuration, where $n > 1$, the electron-electron interaction term arises; therefore, the crystal field splitting turns into significantly complicated. Generally, in the case of RE-doped host materials (known as phosphors), because of the weak crystal field effect, the spin orbit interaction dominates (creates electronic states) and hence generates the ladder-like energy levels of the $4f^n$ valance shell configuration.

Molecular Orbital Theory (MOT) For the interpretation of the molecular electronic structure, MOT is the most important theory discovered by Friedrich Hund, Robert Mulliken, John C. Slater, and John-Lennard Jones (Mulliken 1967). This theory is based on quantum mechanical concepts. For understanding the structure of the energy levels of dopant ions at the quantum level, this theory works as the semi-empirical mode. Besides the GSA, ESA, ETU, and PA processes that are responsible for the generation of UC emission phenomena, the charge transfer mechanism is also an important process. To understand the charge transfer spectra, MOT is useful. In this process, valence electrons are equally shared by the ligand

and the dopant ion (Zhu et al. 2016). Therefore, the eigenfunctions of the molecular orbitals can be written as a direct combination of the eigenfunction of the ligand ion (Ψ_D) plus the eigenfunction of the dopant ion (Ψ_H), i.e.

$$\Psi = C(\Psi_D + \lambda\Psi_H) \quad (1.4)$$

where C is the normalization constant and λ is the mixing coefficient (Solé et al. 2005).

1.4.1.3 Dieke Diagram

The experimental structure of the electronic arrangement of trivalent RE ions is revealed by G. H. Dieke. The triply ionized RE ions can generate spectra (sharp energy levels) while incorporated in any crystal lattice. However, Dieke proved that the transition energies are independent of the host environment. In 1960, Dieke measured the characteristic energy levels (${}^{2S+1}L_J$) of trivalent RE ions doped into LaCl_3 crystal, which is known as the Dieke diagram (Dieke and Crosswhite 1963; Dieke 1968; Dieke and Satten 1970). Since then, this Dieke diagram has become a reference for explaining the energy levels of any trivalent ions doped in any host material.

The extended version of the Dieke diagram has been given by Ogasawara et al. (2004). In Figure 1.5, the width of each and every level indicates the magnitude of the crystal field splitting.

1.4.2 Divalent Rare-Earth Ions

Similar to the trivalent RE ions, divalent RE ions possess a $4f^n$ outer electronic configuration. In the case of divalent RE ions, the $4f^{(n-1)} 5d$ configuration is not distant from the fundamental $4f^n$ configuration. The optical transitions take place from parity-allowed $4f^n \rightarrow 4f^{(n-1)} 5d$ in the case of divalent RE ions. As the transitions are parity allowed, the resultant emission spectra lead to an intense and broad band.

For instance, one of the most important examples of divalent RE ions is Eu^{2+} . Aguilar et al. reported the incorporation of Eu^{2+} ions in NaCl crystal at room temperature (Aguilar et al. 1982). Although Eu^{2+} ions are doped in NaCl crystal, they replace the Na^+ ions, and the spectrum of $\text{Eu}^{2+}:\text{NaCl}$ shows two broad bands analogous to the transition state from the ground state of the $4f^7$ electronic configuration to the excited $4f^6 5d$ transition state. The crystal field yields a splitting of the $5d$ orbital into two components. With the help of X-ray irradiation upon the $\text{Eu}^{2+}:\text{NaCl}$ crystal, Aguilar observed that some Eu^{2+} ions converted into Eu^{3+} ions; hence, additional peaks are observed in the optical spectra. The optical features of the bands show broad and intense band owing to Eu^{2+} ions (parity-allowed transition), while narrow and weak bands are due to the Eu^{3+} ions (parity-forbidden transition). Furthermore, unlike trivalent ions, divalent ions change their optical properties in different host crystal environments.

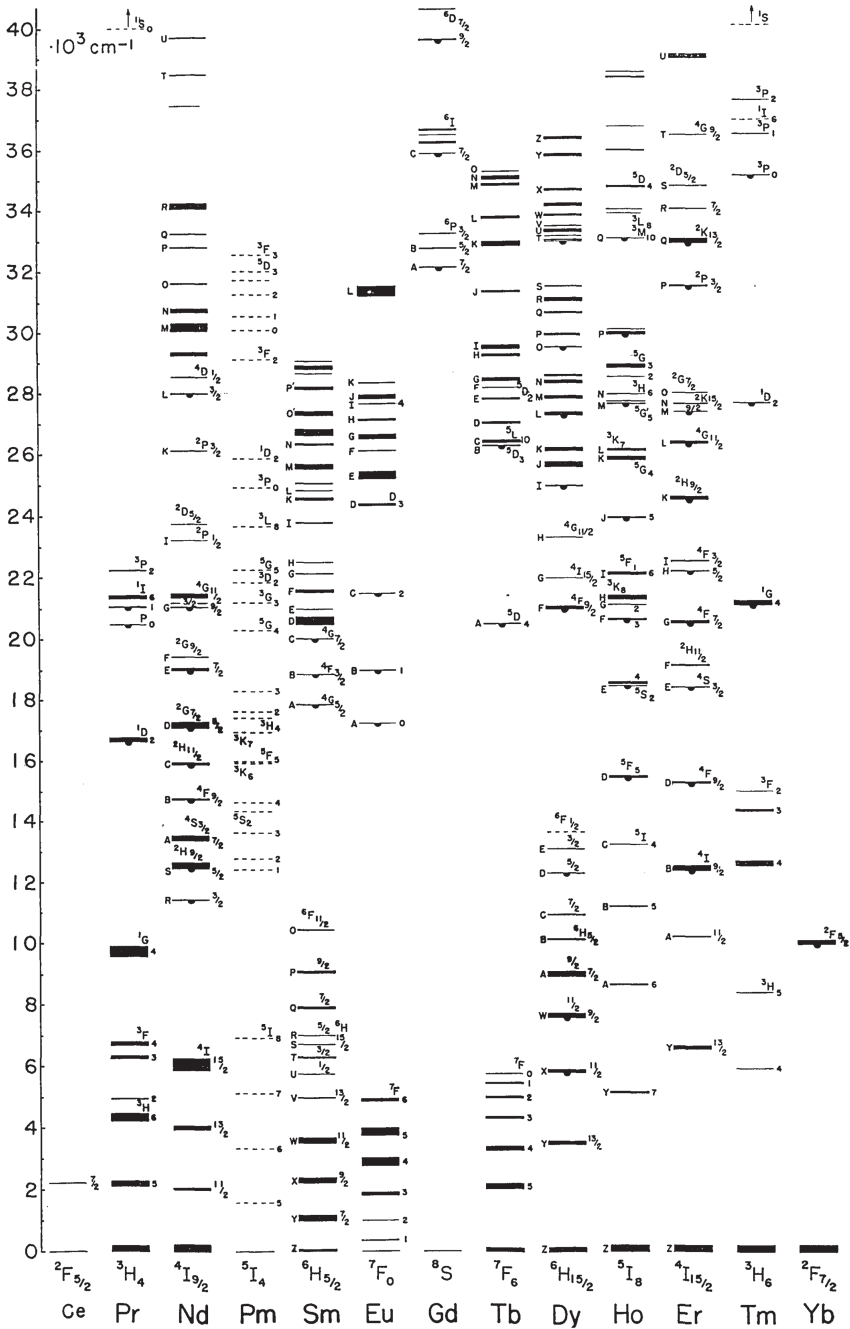


Figure 1.5 Energy levels of the trivalent RE ions. Reprinted with permission from ref. Source: Dieke and Crosswhite (1963). Reprinted with permission of The Optical Society.

1.5 Excitation and De-excitation Processes of Rare Earths in Solid Materials

1.5.1 Excitation Processes

Depending on the suitable excitation process, the divalent and trivalent RE ions are excited through various excitation routes (Shionoya et al. 1998). Specifically, three types of excitation processes occur.

1.5.1.1 f–f Transition

The trivalent RE ions with an outer electronic configuration $5s^2 5p^6 4f^n$ ($n = 1$ to 14) possess f–f transitions (Shionoya et al. 1998). Therefore, the valence electrons present in 4f shells are mainly accountable for optical transitions. According to the Laporte parity selection rule, 4f–4f transitions are forbidden, and they become allowed only in some host environment; hence, the absorption spectra lead to narrow cross sections.

1.5.1.2 f–d Transition

The f–d transition takes place within the 4f and 5d orbitals. In this process, the electrons present in the 4f orbitals get excited in the direction of higher energy orbitals, i.e. 5d orbitals, and the absorption process is represented as $4f^n \rightarrow 4f^{n-1} 5d$. In this case, 4f–5d transitions are parity allowed according to the parity selection rule; hence, the absorption cross section leads to strong and broad type.

1.5.1.3 Charge Transfer Transition

Apart from f–f and f–d transitions, the charge transfer transition is an important transition process to populate the higher energy state of the RE ions (Shionoya et al. 1998). This process is based on the quantum mechanical concept, and it is related with one neighboring ion and one RE ion. In charge transfer transition, the mixing of two eigenfunction results in the transfer of electrons from neighboring ions to the 4f orbitals of RE ions. For instance, the transfer of 2p electrons of the neighboring oxygen ion (O^{-2}) to a 4f orbital of RE ions causes the charge transfer transition to arise. Considering the parity selection rules, these types of transitions are parity-allowed and thus generate broad and intense absorption spectra (Chen et al. 2000, 2004). These three (f–f, f–d, and charge transfer transition) processes are mainly accountable for the excitation process of the RE ions.

1.5.2 Emission Processes

After exciting the RE ions into higher energy state by suitable electromagnetic radiation, they relax to the ground state or low lying levels via some processes. These processes may be radiative or nonradiative in nature.

1.5.2.1 Emission via Radiative Transitions

The sources of radiations in any electromagnetic radiation process are oscillating electric dipole, oscillating magnetic dipole, oscillating electric quadrupole, and so on. Among these radiations, the electric dipole radiation and the magnetic dipole

radiation contribute more. RE ions may be excited via electromagnetic (UV, visible, infrared, etc.) radiation. Thus, the electric dipole radiation and magnetic dipole radiation are responsible for any optical transition or emission. These transitions depend on parity of the initial and final states of the RE ions. The electric dipole transition takes place only when the initial and final states are of opposite parity; conversely, magnetic dipole transition originates if both the states have same parity. In the case of RE-doped phosphor materials, 4f–4f transitions are parity forbidden and become allowed because of the mixing of the wave functions of 4f orbitals and 5d orbitals in the presence of crystal field. These transitions are known as forced electric dipole transitions. The basic theory of 4f–4f transition properties, radiative emission rates, and lifetime of the states has been explained on the basis of Judd–Ofelt theory (Judd 1962; Ofelt 1962).

1.5.2.2 Emission via Nonradiative Transitions

The RE ions have ladder-like energy levels in the presence of host environment. When these ions are excited by the suitable electromagnetic radiation, some transitions lead to radiative, whereas some of them are nonradiative. When an electron relaxes from higher energy state to lower energy state without emitting a photon, then the relaxation process is known as nonradiative transition. Several mechanisms such as multiphonon relaxation, concentration quenching, etc., are involved for nonradiative transition process.

The multiphonon relaxation occurs when the ions in the excited state transfer their excitation energy to the lattice and no light (i.e. photon) emission takes place. The phonons of highest energy and the maximum density of state participate in this process. For possible emission via the multiphonon relaxation process, the maximum phonon energy should be five times the host vibrational energy. Therefore, the phonon energy should be minimum for higher UC emission intensity.

One more emission process via nonradiative transitions is the concentration quenching process. This process occurs when the dopant ion concentration becomes very high. When the concentration of the dopant ions become very high, the distance between the dopant ions seems to be very small. The ion–ion interaction takes place and cross-relaxation occurs. Thus, the excitation energy is lost via nonradiative relaxation. This process generally occurs in a similar type of dopant ions.

1.5.2.3 Energy Transfer Processes

The energy transfer (ET) process occurs in both similar and different ions (Förster 1948; Dexter 1953; Inokuti and Hirayama 1965). The energy transfer process is mainly of two types, radiative and nonradiative. The ET process occurs between the donor–donor or donor–acceptor system. Radiative energy transfer process arises when an excited sensitizer ion radiates a real photon, and this photon is reabsorbed by the activator ion. This type of ET process takes place through the dipole–dipole interaction process in which the energy transfer probability is proportional to $1/R^2$ (Auzel 1980).

The nonradiative energy transfer process occurs when the excited sensitizer ion transfers its excitation energy to an activator ion without emitting a photon.

The theoretical description can be understood by considering the energy transfer between a donor and an acceptor ion. Let donor ions, i.e. sensitizer, are termed as S and acceptor ions, i.e. activator, are termed as A. Under suitable excitation, the sensitizer ion is excited to the upper energy state S^* by absorbing a photon, and when it returns to the ground state, it transfers its energy to the activator ion without photon emission and relaxes to the ground state; then, the activator ion is excited to the higher energy state by the following process: $S^* + A \rightarrow S + A^*$ (where “*” denotes the excited state).

The energy transfer probability between the sensitizer and the activator is given by (Förster 1948)

$$P = \frac{2\pi}{\hbar} |\langle S^*, A | H_{SA} | S, A^* \rangle|^2 \int g_S(\nu) g_A(\nu) d\nu \quad (1.5)$$

where H_{SA} is the interaction Hamiltonian, \hbar is the Planck constant, $g_S(\nu)$ is the emission spectrum of the sensitizer, and $g_A(\nu)$ is the absorption spectrum of the activator.

Energy transfer interaction takes place via the exchange interaction or the electrostatic multipolar interaction. The exchange interaction arises as the distance between the donor (i.e. sensitizer) and acceptor (i.e. activator) ions are exactly adjacent such that charge distribution can exchange; hence, the orbitals of electrons overlap. In this case, S and A lie at a very small distance ($\leq 6\text{\AA}$) to each other. On the other hand, the electrostatic interaction occurs via induced dipole oscillation in which no overlap occurs between the sensitizer and activator ions. The distance concerning the sensitizer and activator ions is enough ($\sim 20\text{\AA}$); therefore, no physical interaction take place among them. The energy transfer probability of electrostatic interaction can be described as (Förster 1948)

$$P = \frac{2\pi}{\hbar} |\langle S^*, A | H_{SA}^{\text{el}} | S, A^* \rangle|^2 \int g_S(\nu) g_A(\nu) d\nu \quad (1.6)$$

where H_{SA}^{el} signifies the electrostatic interaction Hamiltonian.

By considering the dipole–dipole interaction, this probability of energy transfer can be calculated as (Förster 1948)

$$P = \frac{1}{4\pi\epsilon_0} \frac{3\pi\hbar e^4}{n^4 m^2 \nu^2 R^6} f_S f_A \int g_S(\nu) g_A(\nu) d\nu \quad (1.7)$$

where ϵ_0 is the permittivity in vacuum, n is the refractive index, e and m are the charge and mass of electrons, respectively, ν is the wavenumber of the coming transition, R is the distance between the donor and acceptor ions, and f_S and f_A are the oscillator strengths related to sensitizer emission and activator absorption, respectively. The energy transfer probability according to Förster can be written as (Förster 1948)

$$P = \frac{1}{\tau} \left(\frac{R_0}{R} \right)^6 \quad (1.8)$$

where τ is the excited-state lifetime of the sensitizer ion and R_0 is the Förster radius at which half (50%) of the energy of the sensitizer ion is transferred to the activator ion. Therefore, according to this theory, nonradiative energy transfer probability (followed by dipole–dipole interaction) varies as $1/R^6$.

Conversely, according to the Dexter theory, the energy transfer probability can be generalized as (Dexter 1953)

$$P = \frac{1}{\tau} \left(\frac{R_0}{R} \right)^a \quad (1.9)$$

where “ a ” is the positive integer, and for different types of interactions, it has different values. For dipole–dipole interaction, $a = 6$; for dipole–quadrupole interaction, $a = 8$; and for quadrupole–quadrupole interaction, $a = 10$.

1.6 Rate Equations Relevant to UC Mechanism

The rate equations are usually nontrivial for UC mechanisms because it involves different dopant ions for different host matrices. Depending on the dopant ions, the rate equations of UC mechanism differs. The rate equation corresponding to a particular UC phenomenon depends on various parameters such as different involved processes, pump-induced transition routes, energy transfer mechanisms, radiative and nonradiative decays, cross-relaxation processes, etc.

1.6.1 Rate Equations in a Basic Three-Level System

Let us consider a simplified three-level energy system in which GSA, ESA, and ETU processes are involved (Pollnau et al. 2000; Liu 2015; Mahata et al. 2015; Lu et al. 2016; Marciniak et al. 2016; Mondal et al. 2017; Pattnaik and Rai 2021). The population densities for the ground state G, the intermediate state E1, and the upconverting emitting state E2 are N_0 , N_1 , and N_2 respectively (Figure 1.6). In this case, the assumptions are taken as no pump depletion, the population density of the ground state is constant, and the scheme is constantly pumped by the GSA process.

If σ_i is the absorption cross section from some state $|E_i\rangle$, W_i is the relaxation rate for the ETU process, A_i is the rate of spontaneous emission, and ϕ is the pump rate (which is proportional to the incident pump power P), then the rate equation for a basic three-level system can be written as follows (Etchart 2010):

$$\frac{dN_1}{dt} = \phi\sigma_0N_0 - \phi\sigma_1N_1 - 2W_1N_1^2 - A_1N_1 \quad (1.10)$$

$$\frac{dN_2}{dt} = \phi\sigma_1N_1 + W_1N_1^2 - A_2N_2 \quad (1.11)$$

where $\phi\sigma_0N_0$ is the increase in population density for state E1 via the GSA process; on the other hand, the $\phi\sigma_1N_1$, $2W_1N_1^2$, and A_1N_1 terms indicate the reduction in population density of state E1 via ESA, ETU, and spontaneous emission process, respectively. For state E2, the $\phi\sigma_1N_1$ and $W_1N_1^2$ terms refer to the increase in population density through the GSA and ETU processes, respectively. Alternatively, the third term A_2N_2 shows the decrease in population from state E2 via spontaneous emission.

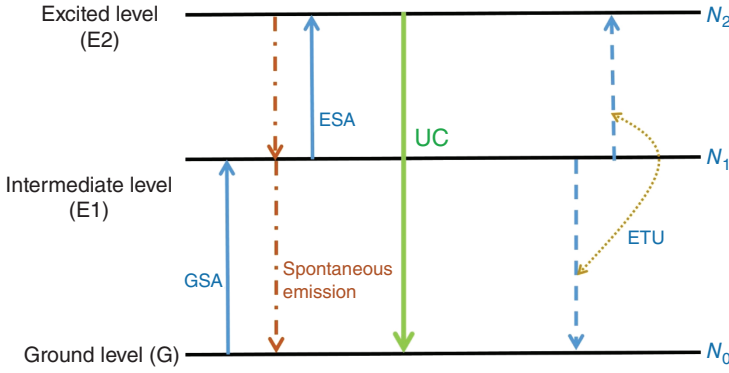


Figure 1.6 Schematic representation of a three-level energy system. The upconversion (UC) mechanism involves GSA, ESA, and ETU processes.

1.6.2 Rate Equation Related to Pump Power-Dependent UC Emission

On the basis of rate equations, the pump power-dependent UC phenomena in both cases, (i) where the ETU mechanism dominates over ESA and (ii) in the case of ESA dominated the UC emission process, can be explained.

Case (i): In the case of ETU-dominating UC emission process from Eqs. (1.10) and (1.11), the ESA, i.e. $\phi\sigma_1N_1$, term can be ignored. The rate equation can be written as

$$\frac{dN_1}{dt} = \phi\sigma_0N_0 - 2W_1N_1^2 - A_1N_1 \quad (1.12)$$

$$\frac{dN_2}{dt} = W_1N_1^2 - A_2N_2 \quad (1.13)$$

Assuming the steady states, Eqs. (1.12) and (1.13) can be equated to zero. Therefore, $\frac{dN_1}{dt} = \phi\sigma_0N_0 - 2W_1N_1^2 - A_1N_1 = 0$, or $\phi\sigma_0N_0 = 2W_1N_1^2 + A_1N_1$, and $\frac{dN_2}{dt} = W_1N_1^2 - A_2N_2 = 0$. For instance, ETU is higher compared to the spontaneous relaxation rate (i.e. $A_1N_1 \ll 2W_1N_1^2$), then $\phi\sigma_0N_0 = 2W_1N_1^2$ or $N_1^2 \propto P_{\text{pump}}$. Also, $W_1N_1^2 = A_2N_2$, then $N_2 \propto N_1^2 \propto P_{\text{pump}}$. Thus, the population density of the upconverting emitting state is proportional to the excitation pump power (P_{pump}) (Dutta 2020). Conversely, when spontaneous relaxation takes over ETU (i.e. $A_1N_1 \gg 2W_1N_1^2$), then $N_1 \propto P_{\text{pump}}$ or $N_2 \propto N_1^2 \propto P_{\text{pump}}^2$. Therefore, in this case, the population density of the emitting state varies as the quadratic power of excitation pump power (P_{pump}).

Case (ii): In the case of ESA-dominating UC emission process, from Eqs. (1.10) and (1.11), the $W_1N_1^2$ term can be ignored. Thus, the rate equations can be written as

$$\frac{dN_1}{dt} = \phi\sigma_0N_0 - \phi\sigma_1N_1 - A_1N_1 \quad (1.14)$$

$$\frac{dN_2}{dt} = \phi\sigma_1N_1 - A_2N_2 \quad (1.15)$$

Under steady-state conditions, Eqs. (1.14) and (1.15) can be equated to zero. As the ESA process dominates over the spontaneous emission rate, i.e. $A_1 N_1 \ll \phi \sigma_1 N_1$, then $N_1 \propto N_2 \propto P_{\text{pump}}$. On the other hand, if the spontaneous rate governs, then $A_1 N_1 \gg \phi \sigma_1 N_1$, thus, $N_1 \propto P_{\text{pump}}$, so $N_2 \propto N_1 \cdot P_{\text{pump}} \propto P_{\text{pump}}^2$.

Thus, while increasing the pump power, when the spontaneous emission rate dominates over ESA, the population density of the emitting state varies quadratically with the excitation pump power.

1.7 Theoretical Description of Optical Characteristics of Rare-Earth Ions

For instance, the electrons when de-excited from state E2 to state E1 give radiative emission; then, the rate of change of population density of N_2 is given by (Etchart 2010)

$$\frac{dN_2}{dt} = -A_T N_2(t) = -(A_r + A_{\text{nr}}) N_2(t) \quad (1.16)$$

where A_T is the overall decay rate of radiative (A_r) and nonradiative (A_{nr}) terms.

The lifetime (experimental) of the upconverting emitting state is given by

$$\tau_{\text{exp}} = \frac{1}{A_r + A_{\text{nr}}} \quad (1.17)$$

Conversely, the quantum efficiency (radiative) can be calculated as

$$\eta_r = \frac{A_r}{A_T} = \frac{A_r}{A_r + A_{\text{nr}}} = \frac{\tau_{\text{exp}}}{\tau_r} \quad (1.18)$$

where τ_r is known as the radiative lifetime.

The optical transition probability can be calculated by using the term $M = \langle \Psi_i | \Gamma_D | \Psi_f \rangle$ where Ψ_i and Ψ_f are the wave functions related to the two initial and final states and Γ_D is the dipole momentum operator. Conferring to the group theory, the transition can be only allowed if $M \neq 0$. As the emitting wave is light wave, i.e. electromagnetic wave, it consists of electric dipole and magnetic dipole transitions. According to the Laporte rule, Ψ_i and Ψ_f must have opposite parities. The conditions for the allowed electric dipole transitions are as follows:

$$\Delta S = 0, \Delta L = \pm 1, \text{ and } \Delta J \leq \pm 6 \text{ (but } J = 0 \rightarrow J' = 0 \text{ are forbidden)}$$

$$J = 0, \Delta L = \pm 1, \text{ and } \Delta J = \pm 2, \pm 4, \pm 6$$

On the other hand, the magnetic dipole operator is an even operator; hence, magnetic dipole transitions will be allowed only if Ψ_i and Ψ_f have the same parities. The conditions for magnetic dipole transitions are

$$\Delta S = 0, \Delta L = 0, \text{ and } \Delta J = 0, \pm 1 \text{ (but } J = 0 \rightarrow J' = 0 \text{ are forbidden)}$$

$$J = 0, \Delta L = 0, \text{ and } \Delta J = \pm 1$$

In rare-earth doped materials, the electric dipole transitions occur because of the forced electric dipole transitions.

1.7.1 Judd–Ofelt (J–O) Theory and Calculation of Radiative Parameters

The theoretical calculation on the intensities of the RE ions has been described by Judd and Ofelt in 1962. This theory gives the information about the transition probability, radiative lifetime, and oscillator strengths as well as the quantum efficiency. Conferring to the Judd–Ofelt theory, the oscillator strength (f) used for the absorption bands analogous to the electronic transition from initial state $^{2S+1}L_J$ to the final state $^{2S'+1}L_{J'}$ can be written as (Rai and Rai 2004; Liu 2005; Mahato et al. 2005; Rai et al. 2006; Etchart 2010; Azam and Rai 2017)

$$f = f_{\text{ED}} + f_{\text{MD}} = \frac{8\pi^2 m c \nu}{3 h e^2 n^2 (2J + 1)} (\chi_{\text{ED}} S_{\text{ED}} + \chi_{\text{MD}} S_{\text{MD}}) \quad (1.19)$$

where m and e denote the mass and charge of electron, respectively, ν is the wavenumber related to the observed transition, c is the speed of light, n is the refractive index of the host, S_{ED} and S_{MD} are the electric dipole line strength and magnetic dipole line strength of the electronic transition, respectively, and χ is the local field correction due to the crystal field effect of the host.

The local field correction factor and the line strength for electric dipole transition can be calculated as (Rai and Rai 2004; Mahato et al. 2005; Rai et al. 2006; Azam and Rai 2017)

$$\chi_{\text{ED}} = n \left(\frac{n^2 + 2}{3} \right)^2 \quad (1.20)$$

$$S_{\text{ED}} = e^2 \sum_{t=2,4,6} \Omega_t |\langle (S, L)J || U^{(t)} || (S', L')J' \rangle|^2 \quad (1.21)$$

Equally, the parameter local field correction and line strength for magnetic dipole transition can be written as

$$\chi_{\text{MD}} = n^3 \quad (1.22)$$

$$S_{\text{MD}} = \mu_{\text{B}}^2 |\langle (S, L)J || L + 2S || (S', L')J' \rangle|^2 \quad (1.23)$$

where μ_{B} denotes the Bohr magneton.

The Judd–Ofelt intensity parameters are Ω_2 , Ω_4 , and Ω_6 . Carnall and Kaminskii (Carnall et al. 1968; Kaminskii 1990) described the value of reducible matrix element $|\langle (S, L)J || U^{(t)} || (S', L')J' \rangle|$, which depends on the crystal field effect of the host for different RE ions.

The spontaneous decay rate can be determined as (Liu 2005; Etchart 2010)

$$A_{\text{r}} = A_{\text{ED}} + A_{\text{MD}} = \frac{64\pi^4 \nu^3}{3h(2J + 1)} (\chi_{\text{ED}} S_{\text{ED}} + \chi_{\text{MD}} S_{\text{MD}}) \quad (1.24)$$

This radiative term strongly depends on the energy gap of the two involved electronic states, the higher the energy gap, the higher the radiative emission rate.

The radiative lifetime can be calculated as

$$\tau_{\text{r}} = \frac{1}{\sum_J A_{\text{r}}(J' \rightarrow J)} \quad (1.25)$$

1.7.2 Nephelauxetic Effect

In the inorganic materials, a metal ion is encircled by ligands, which modifies the electron surroundings of the metal ion. When the ligands bind to a metal ion, the metal ion orbitals spread out because of the delocalization of electrons. The spreading out of the electron cloud is known as the nephelauxetic effect (Jørgensen 1962, Luo et al. 2010; Som et al. 2015, Mukhopadhyay and Rai 2018; Azam and Rai 2019). As a consequence, the energy needed for pairing of electrons in metal ions is smaller than the energy required in the case of free ions. For metal ions, Racah parameters can be governed by the nature of the ligand ions attached to the metal ion. In the case of lanthanide ion-doped materials, the nature of bonding between the RE ions and their surrounding oxygen atoms may be studied from the absorption spectra. The slight variations in the peak positions of the absorption bands in all the RE ion-doped materials arise because of the variation in the environment around the RE ions on complexation. Also, the deviation in the positions of absorption bands arises because of the expansion of the partially filled 4f shells.

The nephelauxetic ratio (β^-) can be mathematically expressed by using the following relation (Luo et al. 2010; Som et al. 2015; Mukhopadhyay and Rai 2018; Azam and Rai 2019):

$$\beta^- = \frac{1}{n} \sum \frac{\nu_{\text{complex}}}{\nu_{\text{free ion}}} \quad (1.26)$$

where ν is the wavenumber of absorption band transition in the corresponding material and “ n ” is the number of the observed absorption transitions.

The covalency (δ) and the bonding parameters ($b^{1/2}$) can be calculated by using the following expressions (Mukhopadhyay and Rai 2018; Azam and Rai 2019):

$$\delta = \left[\frac{1 - \beta^-}{\beta^-} \right] \quad (1.27)$$

$$\text{and } b^{1/2} = \left[\frac{1 - \beta^-}{2} \right]^{1/2} \quad (1.28)$$

The positive or negative value of “ δ ” explains the covalent or ionic nature of bonding between the RE ions and their surrounding oxygen atoms.

1.8 An Introduction to Upconverting Nanoparticles

Generally, UCNPs with a size less than or equal to 100 nm consist of a host and an optically active center where dopants (e.g. RE ions) act as the optical center. Despite promising results achieved from luminescent materials such as organic dyes and quantum dots, their weak photostability and broad absorption and emission bands with moderate quantum yield restrict their various practical applications (Cheng et al. 2011). UCNPs play an effective role in modern days because of their nonblinking property, long lifetime, high chemical stability, sharp emission bands, large anti-Stokes shift, etc. (Wang et al. 2011; Chen et al. 2014; Mondal et al. 2017; Shao et al. 2018; Soni et al. 2019). The emission characteristics of these UCNPs differ with the selection of different dopants, hosts, excitation wavelengths, etc. In the UCNPs

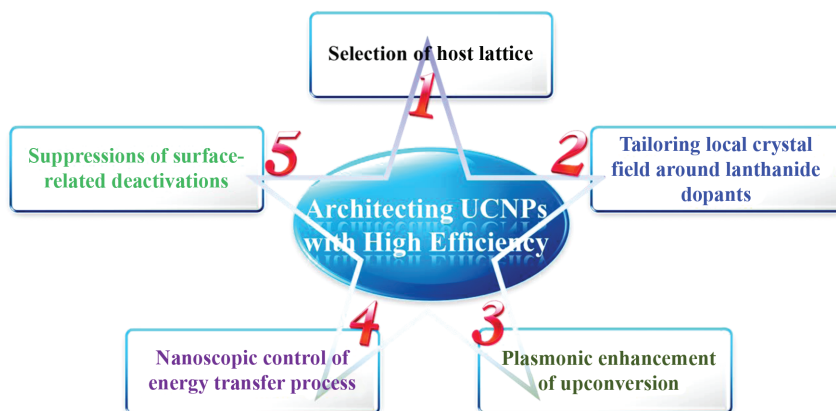


Figure 1.7 General strategies to achieve the high efficiency of UCNPs. Source: Chen et al. (2014). Reprinted with permission of American Chemical Society.

containing RE ions, the emission features, because of the shielded 4f–4f orbital electronic transitions, are not influenced greatly by the host NPs or bulk materials. However, the host with nanometer size plays an important and unique role in enhancing the UC emission intensity and emission profile. Figure 1.7 describes the general strategies to achieve the high efficiency of UCNPs. Primarily, a host material with low vibrational energy is essential to minimize the energy loss because of the nonradiation effect and hence improves the radiative UC emission property.

For nanoparticles, owing to their high surface-to-volume ratio, the dopant ions present near the surface of nanoparticles lose their emission properties by surface quenching centers and hence decrease the UC efficiency. For this, the different surface engineering approaches in UCNPs have been developed (Figure 1.7), such as homogeneous core@shell structure, heterogeneous core@shell structure, active core/active shell structure, plasmonic UCNPs, etc., to enhance the conversion efficiency (Chen et al. 2014; Fan et al. 2014; Mondal et al. 2017; Shao et al. 2018; Soni et al. 2019; Sui et al. 2019).

Acknowledgments

Authors are grateful to the Council of Scientific and Industrial Research (CSIR), New Delhi, India, project no. 03(1354)/16/EMR-II, for providing financial assistance in the form of a research project.

References

- Aguilar, M., García Solé, G.J., H. Murrieta, S. et al. (1982). Trivalent europium in x-irradiated NaCl: Eu. *Physical Review B* 26: 4507. <https://doi.org/10.1103/physrevb.26.4507>.

- Auzel, F. (1966). Quantum counter by energy transfer between two rare earth ions in a mixed tungstate and in a glass. *Comptes Rendus de l'Académie des Sciences (Paris)* 262: 1016.
- Auzel, F.E. (1973). Materials and devices using double-pumped-phosphors with energy transfer. *Proceedings of the IEEE* 6: 758–786. <https://doi.org/10.1109/proc.1973.9155>.
- Auzel, F. (1980). Multiphonon processes, cross-relaxation and up-conversion in ion-activated solids, exemplified by minilaser materials. In: *Radiationless Processes*, 213–286. https://doi.org/10.1007/978-1-4613-3174-2_6.
- Auzel, F. (2004). Upconversion and anti-Stokes processes with f and d ions in solids. *Chemical Reviews* 104: 139–174. <https://doi.org/10.1021/cr020357g>.
- Azam, M. and Rai, V.K. (2017). Ho³⁺-Yb³⁺ codoped tellurite based glasses in visible lasers and optical devices: Judd–Ofelt analysis and frequency upconversion. *Solid State Sciences* 66: 7–15. <https://doi.org/10.1016/j.solidstatesciences.2017.02.001>.
- Azam, M. and Rai, V.K. (2019). Effect of the addition of Pb₃O₄ and TiO₂ on the optical properties of Er³⁺/Yb³⁺:TeO₂–WO₃ glasses. *ACS Omega* 4: 16280–16291. <https://doi.org/10.1021/acsomega.9b00609>.
- Berthou, H. and Jörgensen, C.K. (1990). Optical-fiber temperature sensor based on upconversion-excited fluorescence. *Optics Letters*. <https://doi.org/10.1364/ol.15.001100>.
- Boyer, J.C., Cuccia, L.A., and Capobianco, J.A. (2007). Synthesis of colloidal upconverting NaYF₄:Er³⁺/Yb³⁺ and Tm³⁺/Yb³⁺ monodisperse nanocrystals. *Nano Letters* 7: 847–852. <https://doi.org/10.1021/nl070235+>.
- Brik, M.G., Camardello, S.J., Srivastava, A.M. et al. (2016). Spin-forbidden transitions in the spectra of transition metal ions and nephelauxetic effect. *ECS Journal of Solid State Science and Technology* 5: R3067–R3077. <https://doi.org/10.1149/2.0091601jss>.
- Carnall, W.T., Fields, P.R., and Rajnak, K. (1968). Spectral intensities of the trivalent lanthanides and actinides in solution. II. Pm³⁺, Sm³⁺, Eu³⁺, Gd³⁺, Tb³⁺, Dy³⁺, and Ho³⁺. *The Journal of Chemical Physics* 49: 4412–4423. <https://doi.org/10.1063/1.1669892>.
- Carnall, W.T., Goodman, G.L., Rajnak, K. et al. (1989). A systematic analysis of the spectra of the lanthanides doped into single crystal LaF₃. *The Journal of Chemical Physics* 90: 3443–3457. <https://doi.org/10.1063/1.455853>.
- Chen, W., Malm, J.O., Zwiller, V. et al. (2000). Energy structure and fluorescence of Eu²⁺ in ZnS:Eu nanoparticles. *Physical Review B* 61: 11021–11024. <https://doi.org/10.1103/physrevb.61.11021>.
- Chen, W., Joly, A.G., Malm, J.O. et al. (2004). Upconversion luminescence of Eu³⁺ and Mn²⁺ in ZnS:Mn²⁺, Eu³⁺ codoped nanoparticles. *Journal of Applied Physics* 95: 667–672. <https://doi.org/10.1063/1.1633345>.
- Chen, G.Y., Qju, H.L., Prasad, P.N. et al. (2014). Upconversion nanoparticles: design, nanochemistry, and applications in theranostics. *Chemical Reviews* 114: 5161–5214. <https://doi.org/10.1021/cr400425h>.
- Chen, X., Peng, D., Ju, Q. et al. (2015). Photon upconversion in core–shell nanoparticles. *Chemical Society Reviews* 44: 1318. <https://doi.org/10.1039/c4cs00151f>.
- Cheng, L., Yang, K., Li, Y. et al. (2011). Facile preparation of multifunctional upconversion nanoprobe for multimodal imaging and dual-targeted photothermal

- therapy. *Angewandte Chemie International Edition* 50: 7385–7390. <https://doi.org/10.1002/anie.201101447>.
- Cheng, L., Wang, C., and Liu, Z. (2013). Upconversion nanoparticles and their composite nanostructures for biomedical imaging and cancer therapy. *Nanoscale* 5: 23–37. <https://doi.org/10.1039/C2NR32311G>.
- Chivian, J.S., Case, W.E., and Eden, D.D. (1979). The photon avalanche: a new phenomenon in Pr^{3+} based infrared quantum counters. *Applied Physics Letters* 35: 124. <https://doi.org/10.1063/1.91044>.
- Dexter, D.L. (1953). A theory of sensitized luminescence in solids. *The Journal of Chemical Physics* 21: 836–850. <https://doi.org/10.1063/1.1699044>.
- Dey, R. and Rai, V.K. (2017). Er^{3+} - Tm^{3+} - Yb^{3+} : CaMoO_4 phosphor as an outstanding upconversion-based optical temperature sensor and optical heater. *Methods and Applications in Fluorescence* <https://doi.org/10.1088/2050-6120/aa5e31>.
- Diaz-Torres, L.A., De la Rosa, E., Salas, P. et al. (2005). Enhanced cooperative absorption and upconversion in Yb^{3+} doped YAG nanophosphors. *Optical Materials* 27: 1305–1310. <https://doi.org/10.1016/j.optmat.2004.10.020>.
- Dieke, G.H. (1968). *Spectra and Energy Levels of Rare-Earth Ions in Crystals*, vol. 261, 263. New York: Wiley-Interscience.
- Dieke, G.H. and Crosswhite, H.M. (1963). The spectra of the doubly and triply ionized rare earths. *Applied Optics* 2: 675–686. <https://doi.org/10.1364/ao.2.000675>.
- Dieke, G.H. and Satten, R.A. (1970). Spectra and energy levels of rare earth ions in crystals. *American Journal of Physics* 38: 399–400. <https://doi.org/10.1119/1.1976350>.
- Dignonnet, M.J.F. (1993). *Rare Earth Doped Fiber Lasers and Amplifier*. New York: Dekker. <https://doi.org/10.1201/9780203904657>.
- Dutta, J. (2020). Preparation and characterization of lanthanides doped Yttrium based materials for multifunctional applications. Doctoral thesis. IIT(SM) Dhanbad.
- Dwivedi, Y., Thakur, S.N., and Rai, S.B. (2007). Study of frequency upconversion in $\text{Yb}^{3+}/\text{Eu}^{3+}$ by cooperative energy transfer in oxyfluoroborate glass matrix. *Applied Physics B* 89: 45–51. <https://doi.org/10.1007/s00340-007-2747-y>.
- Etchart, I. (2010). Metal oxides for efficient infrared to visible upconversion. Doctoral thesis. University of Cambridge.
- Fan, W., Shen, B., Bu, W. et al. (2014). A smart upconversion-based mesoporous silica nanotheranostic system for synergetic chemo-/radio-/photodynamic therapy and simultaneous MR/UCL imaging. *Biomaterials* 35: 8992. <https://doi.org/10.1016/j.biomaterials.2014.07.024>.
- Förster, T. (1948). Intermolecular energy migration and fluorescence. *Annalen der Physik* 437: 55–75. <https://doi.org/10.1002/andp.19484370105>.
- Franken, P.A., Weinreich, G., Peters, C.W. et al. (1961). Generation of optical harmonics. *Physical Review Letters* 7: 118–119. <https://doi.org/10.1103/physrevlett.7.118>.
- Gamelin, D.R. and Gudel, H.U. (2000). Design of luminescent inorganic materials: new photophysical processes studied by optical spectroscopy. *Accounts of Chemical Research* 33: 235–242. <https://doi.org/10.1021/ar990102y>.
- Garlick, G.F.J. (1976). Infrared to visible light conversion. *Contemporary Physics* 17: 127–144. <https://doi.org/10.1080/00107517608210848>.

- Grzybowski, A. and Pietrzak, K. (2013). Maria Goeppert-Mayer (1906–1972): two-photon effect on dermatology. *Clinics in Dermatology* 31: 221–225. <https://doi.org/10.1016/j.clindermatol.2012.06.002>.
- Gu, Z.J., Yan, L., Tian, G. et al. (2013). Recent advances in design and fabrication of upconversion nanoparticles and their safe theranostic applications. *Advanced Materials* 25: 3758–3779. <https://doi.org/10.1002/adma.201301197>.
- Heer, S., Lehmann, O., Haase, M. et al. (2003). Blue, green, and red upconversion emission from lanthanide-doped LuPO₄ and YbPO₄ nanocrystals in a transparent colloidal solution. *Angewandte Chemie International Edition* 42: 3179–3182. <https://doi.org/10.1002/anie.200351091>.
- Huang, X., Sanyang Han, S., Huang, W. et al. (2013). Enhancing solar cell efficiency: the search for luminescent materials as spectral converters. *Chemical Society Reviews* 42: 173–201. <https://doi.org/10.1039/C2CS35288E>.
- Inokuti, M. and Hirayama, F. (1965). Influence of energy transfer by the exchange mechanism on donor luminescence. *The Journal of Chemical Physics* 43: 1978–1989. <https://doi.org/10.1063/1.1697063>.
- Jablonski, A. (1935). About the mechanism of photo-luminescence of dye phosphors. *Zeitschrift für Angewandte Physik* 94: 38–46. <https://doi.org/10.1007/bf01330795>.
- Jablonski, A. (1993). Efficiency of anti-Stokes fluorescence in dyes. *Nature* 131: 839–840. <https://doi.org/10.1038/131839b0>.
- Jiang, G., Zhou, S., Wei, X. et al. (2016). 794 nm excited core-shell upconversion nanoparticles for optical temperature sensing. *RSC Advances* 6: 11795–11801. <https://doi.org/10.1039/C5RA27203C>.
- Jørgensen, C.K. (1962). The nephelauxetic series. In: *Progress in Inorganic Chemistry*, vol. 4, 73–124. Wiley <https://doi.org/10.1002/9780470166055.ch2>.
- Joubert, M.F. (1999). Photon avalanche upconversion in rare earth laser materials. *Optical Materials* 11: 181–203. [https://doi.org/10.1016/s0925-3467\(98\)00043-3](https://doi.org/10.1016/s0925-3467(98)00043-3).
- Judd, B.R. (1962). Optical absorption intensities of rare-earth ions. *Physical Review* 127: 750–761. <https://doi.org/10.1103/physrev.127.750>.
- Kaminskii, A.A. (1990). *Laser Crystals, Their Physics and Properties*. New York/Berlin/Heidelberg: Springer. <https://doi.org/10.1007/978-3-540-70749-3>.
- König, E. and Kremer, S. (1997). *Ligand Field Energy Diagrams*. New York: Plenum Press.
- Lee, L.S., Rand, S.C., and Schawlow, A.L. (1984). Cooperative energy transfer among Pr³⁺ ions in LaF₃. *Physical Review B* 29: 6901–6906. <https://doi.org/10.1103/physrevb.29.6901>.
- Li, X., Wang, R., Zhang, F. et al. (2013). Nd³⁺ sensitized up/down converting dual-mode nanomaterials for efficient in-vitro and in-vivo bioimaging excited at 800 nm. *Scientific Reports* 3: 3536. <https://doi.org/10.1038/srep03536>.
- Liang, H.J., Chen, G.Y., Li, L. et al. (2009). Upconversion luminescence in Yb³⁺/Tb³⁺-codoped monodisperse NaYF₄ nanocrystals. *Optics Communications* 282: 3028–3031. <https://doi.org/10.1016/j.optcom.2009.04.006>.
- Lin, C.C., Meijerink, A., and Liu, R.S. (2016). Critical red components for next-generation white LEDs. *The Journal of Physical Chemistry Letters* 7: 495–503. <https://doi.org/10.1021/acs.jpcclett.5b02433>.

- Liu, G. (2005). *Electronic Energy Level Structure*, Springer Series in Materials Science, 1–94. Springer. https://doi.org/10.1007/3-540-28209-2_1.
- Liu, G. (2015). Advances in the theoretical understanding of photon upconversion in rare-earth activated nanophosphors. *Chemical Society Reviews* 44: 1635. <https://doi.org/10.1039/c4cs00187g>.
- Loo, J.F.C., Chien, Y.H., Yin, F. et al. (2019). Upconversion and downconversion nanoparticles for biophotonics and nanomedicine. *Coordination Chemistry Reviews* 400: 213042. <https://doi.org/10.1016/j.ccr.2019.213042>.
- Lu, H., Meng, R., Hao, H. et al. (2016). Stark sublevels of Er^{3+} - Yb^{3+} codoped $\text{Gd}_2(\text{WO}_4)_3$ phosphor for enhancing the sensitivity of a luminescent thermometer. *RSC Advances* 6: 57667. <https://doi.org/10.1039/c6ra10138k>.
- Luo, W., Liao, J., Lia, R. et al. (2010). Determination of Judd–Ofelt intensity parameters from the excitation spectra for rare-earth doped luminescent materials. *Physical Chemistry Chemical Physics* 12: 3276. <https://doi.org/10.1039/b921581f>.
- Maciel, G.S., Biswas, A., Kapoor, R., and Prasad, P.N. (2000). Blue cooperative upconversion in Yb^{3+} -doped multicomponent sol-gel-processed silica glass for three-dimensional display. *Applied Physics Letters* 76: 1978–1980. <https://doi.org/10.1063/1.126228>.
- Mahata, M.K., Kumar, K., and Rai, V.K. (2015). Er^{3+} - Yb^{3+} doped vanadate nanocrystals: a highly sensitive thermographic phosphor and its optical nanoheater behavior. *Sensors and Actuators B* 209: 775–780. <https://doi.org/10.1016/j.snb.2014.12.039>.
- Mahato, K.K., Rai, A., and Rai, S.B. (2005). Optical properties of Dy^{3+} doped in oxyfluoroborate glass. *Spectrochimica Acta Part A* 61: 431–436. <https://doi.org/10.1016/j.saa.2004.02.038>.
- Marciniak, L., Waszniewska, K., Bednarkiewicz, A. et al. (2016). Sensitivity of a nanocrystalline luminescent thermometer in high and low excitation density regimes. *Journal of Physical Chemistry C* 120: 8877–8882. <https://doi.org/10.1021/acs.jpcc.6b01636>.
- Martí n, I.R., Yanes, A.C., Méndez-Ramos, J. et al. (2001). Cooperative energy transfer in Yb^{3+} - Tb^{3+} codoped silica sol-gel glasses. *Journal of Applied Physics* 89: 2520–2524. <https://doi.org/10.1063/1.1344216>.
- Mehra, S., Bishnoi, S., Jaiswal, A. et al. (2020). A review on spectral converting nanomaterials as a photoanode layer in dye-sensitized solar cells with implementation in energy storage devices. *Energy Storage* 2: 1–28. <https://doi.org/10.1002/est2.120>.
- Mondal, M. and Rai, V.K. (2020). Optical thermometry using stark sublevels in charge compensated transition metal molybdate upconverting phosphors. *Journal of Optics and Laser Technology* 130: 106341. <https://doi.org/10.1016/j.optlastec.2020.106341>.
- Mondal, M., Rai, V.K., Srivastava, C. et al. (2016). Enhanced frequency upconversion in $\text{Ho}^{3+}/\text{Yb}^{3+}/\text{Li}^{+}:\text{YMoO}_4$ nanophosphors for photonic and security ink applications. *Journal of Applied Physics* 120: 233101. <https://doi.org/10.1063/1.4971966>.
- Mondal, M., Rai, V.K., and Srivastava, C. (2017). Influence of silica surface coating on optical properties of Er^{3+} - $\text{Yb}^{3+}:\text{YMoO}_4$ upconverting nanoparticles. *Chemical Engineering Journal* 327: 838–848. <https://doi.org/10.1016/j.cej.2017.06.166>.

- Mukhopadhyay, L. and Rai, V.K. (2018). Investigation of photoluminescence properties, Judd–Ofelt analysis, luminescence nanothermometry and optical heating behaviour of $\text{Er}^{3+}/\text{Eu}^{3+}/\text{Yb}^{3+}:\text{NaZnPO}_4$ nanophosphors. *New Journal of Chemistry* 42: 13122–13134. <https://doi.org/10.1039/C8NJ02320D>.
- Mukhopadhyay, L. and Rai, V.K. (2020). Thermally stable red emitting xenotime phosphate nanophosphors for displays. *Materials Research Bulletin* 121: 110628. <https://doi.org/10.1016/j.materresbull.2019.110628>.
- Mulliken, R.S. (1967). Spectroscopy, molecular orbitals, and chemical bonding. *Science* 157: 13–24. <https://doi.org/10.1126/science.157.3784.13>.
- Nadort, A., Zhao, J., and Goldys, E.M. (2016). Lanthanide upconversion luminescence at the nanoscale: fundamentals and optical properties. *Nanoscale* 8: 13099–13130. <https://doi.org/10.1039/C5NR08477F>.
- Ofelt, G.S. (1962). Intensities of crystal spectra of rare-earth ions. *The Journal of Chemical Physics* 37: 511–520. <https://doi.org/10.1063/1.1701366>.
- Ogasawara, K., Watanabe, S., Sakai, Y. et al. (2004). Calculations of complete $4f^n$ and $4f^{n-1} 5d^1$ energy level schemes of free trivalent rare-earth ions. *Japanese Journal of Applied Physics* 43: L611–L613. Available at: <https://doi.org/10.1143/jjap.43.l611>.
- Ovsyakin, V.V. and Feofilov, P.P. (1966). Cooperative sensitization of luminescence in crystals activated with rare earth ions. *Soviet Journal of Experimental and Theoretical Physics Letters* 4: 317.
- Pattnaik, S. and Rai, V.K. (2020). Impact of charge compensation on optical and thermometric behaviour of titanate phosphors. *Materials Research Bulletin* 125: 110761. <https://doi.org/10.1016/j.materresbull.2019.110761>.
- Pattnaik, S. and Rai, V.K. (2021). Insight into the spectroscopic and thermometric properties of titanate phosphors via a novel co-excited laser system. *Materials Science and Engineering B* 272: 115318. <https://doi.org/10.1016/j.mseb.2021.115318>.
- Pollnau, M., Gamelin, D.R., Lüthi, S.R. et al. (2000). Power dependence of upconversion luminescence in lanthanide and transition-metal-ion systems. *Physical Review B* 61: 3337–3346. <https://doi.org/10.1103/physrevb.61.3337>.
- Rai, V.K. (2007). Temperature sensors and optical sensors. *Applied Physics B* 88: 297–303. <https://doi.org/10.1007/s00340-007-2717-4>.
- Rai, V.K., de Menezes, L.S., and de Araújo, C.B. (2007). Stokes luminescence and frequency upconversion in Pr^{3+} doped TeO_2 – PbO glass. *Journal of Applied Physics* 101: 123514. <https://doi.org/10.1063/1.2745314>.
- Rai, V.K. and Rai, S.B. (2004). Optical transitions of Dy^{3+} in tellurite glass: observation of upconversion. *Solid State Communications* 132: 647–652. <https://doi.org/10.1016/j.ssc.2004.07.067>.
- Rai, V.K., Rai, S.B., and Rai, D.K. (2006). Optical studies of Dy^{3+} doped tellurite glass: Observation of yellow-green upconversion. *Optics Communications* 257: 112–119. <https://doi.org/10.1016/j.optcom.2005.07.022>.
- Rai, V.K., de Araújo, C.B., Ledemi, Y. et al. (2008). Frequency upconversion in a Pr^{3+} doped chalcogenide glass containing silver nanoparticles. *Journal of Applied Physics* 103: 103526. <https://doi.org/10.1063/1.2927402>.
- Rai, V.K., Pandey, A., and Dey, R. (2013). Photoluminescence study of $\text{Y}_2\text{O}_3:\text{Er}^{3+}-\text{Eu}^{3+}-\text{Yb}^{3+}$ phosphor for lighting and sensing applications. *Journal of*

- Applied Physics* 113: 083104. <http://link.aip.org/link/doi/10.1063/1.4793265?ver=pdfcov>.
- Reddy, K.L., Balaji, R., Kumar, A. et al. (2018). Lanthanide doped near infrared active upconversion nanophosphors: Fundamental concepts, synthesis strategies, and technological applications. *Small* 14: 1801304. <http://dx.doi.org/10.1002/sml.201801304>.
- Salley, G.M., Valiente, R., and Gudel, H.U. (2001). Luminescence upconversion mechanisms in Yb^{3+} - Tb^{3+} systems. *Journal of Luminescence* 94: 305–309. [https://doi.org/10.1016/s0022-2313\(01\)00310-6](https://doi.org/10.1016/s0022-2313(01)00310-6).
- Salley, G.M., Valiente, R., and Güdel, H.U. (2003). Cooperative Yb^{3+} - Tb^{3+} dimer excitations and upconversion in $\text{Cs}_3\text{Tb}_2\text{Br}_9$: Yb^{3+} . *Physical Review B* 67: <https://doi.org/10.1103/physrevb.67.134111>.
- Shan, J., Qin, X., Yao, N. et al. (2007). Synthesis of monodisperse hexagonal NaYF_4 :Yb, Ln (Ln = Er, Ho and Tm) upconversion nanocrystals in TOPO. *Nanotechnology* 18: 445607. <https://doi.org/10.1088/0957-4484/18/44/445607>.
- Shao, Q., Yang, Z., Zhang, G. et al. (2018). Multifunctional lanthanide-doped core/shell nanoparticles: integration of upconversion luminescence, temperature sensing, and photothermal conversion properties. *ACS Omega* 3: 188–197. <https://doi.org/10.1021/acsomega.7b01581>.
- Shionoya, S., and Yen, W.M. (eds.) 1998. *Phosphor Handbook*, CRC Press, Boca Raton, Florida.
- Singh, A.K., Kumar, K., Pandey, A.C. et al. (2011). Photon avalanche upconversion and pump power studies in LaF_3 : Er^{3+} / Yb^{3+} phosphor. *Applied Physics B* 104: 1035–1041. <https://doi.org/10.1007/s00340-011-4673-2>.
- Solé, J.G., Bausá, L.E., and Jaque, D. (2005). Applications: rare earth and transition metal ions, and color centers. In: *An Introduction to the Optical Spectroscopy of Inorganic Solids*, 199–234. Wiley <https://doi.org/10.1002/0470016043>.
- Som, S., Das, S., Dutta, S. et al. (2015). Synthesis of strong red emitting Y_2O_3 : Eu^{3+} phosphor by potential chemical routes: comparative investigations on the structural evolutions, photometric properties and Judd–Ofelt analysis. *RSC Advances* 5: 70887. <https://doi.org/10.1039/c5ra13247a>.
- Soni, A.K., Dey, R., and Rai, V.K. (2015). Stark sublevels in Tm^{3+} - Yb^{3+} codoped $\text{Na}_2\text{Y}_2\text{B}_2\text{O}_7$ nanophosphor for multifunctional applications. *RSC Advances* 5: 34999–35009. <https://doi.org/10.1039/C4RA15891A>.
- Soni, A.K., Joshi, R., Singh, B.P. et al. (2019). Near-infrared- and magnetic-field-responsive NaYF_4 : Er^{3+} / Yb^{3+} @ SiO_2 @ AuNP @ Fe_3O_4 nanocomposites for hyperthermia applications induced by fluorescence resonance energy transfer and surface plasmon absorption. *ACS Applied Nano Materials* 2: 7350–7361. <https://doi.org/10.1021/acsnm.9b01867>.
- Sui, J., Chen, Z., Liu, G. et al. (2019). Multifunctional Ag @ NaGdF_4 : Yb^{3+} , Er^{3+} core-shell nanocomposites for dual-mode imaging and photothermal therapy. *Journal of Luminescence* 209: 357–364. <https://doi.org/10.1016/j.jlumin.2019.01.046>.
- Suijver, J.F. (2008). *Luminescence: From Theory to Applications*, ch. 6 (ed. C. Ronda), 134. Weinheim: Wiley-VCH Verlag GmbH and Co. KGaA.

- Tanabe, Y. and Sugano, S. (1954a). On the absorption spectra of complex ions I. *Journal of the Physical Society of Japan* 9: 753–766. <https://doi.org/10.1143/jpsj.9.753>.
- Tanabe, Y. and Sugano, S. (1954b). On the absorption spectra of complex ions II. *Journal of the Physical Society of Japan* 9: 766–779. <https://doi.org/10.1143/jpsj.9.766>.
- Tanabe, Y. and Sugano, S. (1956). On the absorption spectra of complex ions, III. The calculation of the crystalline field strength. *Journal of the Physical Society of Japan* 11: 864–877. <https://doi.org/10.1143/jpsj.11.864>.
- Wade, S.A., Collins, S.F., and Baxter, G.W. (2003). Fluorescence intensity ratio technique for optical fiber point temperature sensing. *Journal of Applied Physics* 94: 4743–4756. <https://doi.org/10.1063/1.1606526>.
- Wang, F. and Liu, X.G. (2009). Recent advances in the chemistry of lanthanide-doped upconversion nanocrystals. *Chemical Society Reviews* 38: 976–989. <https://doi.org/10.1039/b809132n>.
- Wang, R. and Zhang, F. (2014). NIR luminescent nanomaterials for biomedical imaging. *Journal of Materials Chemistry B* 2: 2422–2443. <https://doi.org/10.1039/c3tb21447h>.
- Wang, M., Abbineni, G., Clevenger, A. et al. (2011). Upconversion nanoparticles: synthesis, surface modification and biological applications. *Nanomedicine: Nanotechnology, Biology and Medicine* 7: 710–729. <https://doi.org/10.1016/j.nano.2011.02.013>.
- Wybourne, B.G. (1965). *Spectroscopic Properties of Rare Earths*. New York: Wiley.
- Wybourne, B.G. and Meggers, W.F. (1965). Spectroscopic properties of rare earths. *Physics Today* 18: 70–72. <https://doi.org/10.1063/1.3047727>.
- You, M., Lin, M., Wang, S. et al. (2016). Three-dimensional quick response code based on inkjet printing of upconversion fluorescent nanoparticles for drug anti-counterfeiting. *Nanoscale* 8: 10096. <https://doi.org/10.1039/c6nr01353h>.
- Zhu, Y., Xu, W., Li, C. et al. (2012). Broad white light and Infrared emission bands in $\text{YVO}_4:\text{Yb}^{3+}, \text{Ln}^{3+}$ ($\text{Ln}^{3+} = \text{Er}^{3+}, \text{Tm}^{3+}$ or Ho^{3+}). *Applied Physics Express* 5: 092701. <https://doi.org/10.1143/APEX.5.092701>.
- Zhu, S., Wang, C., Li, Z. et al. (2016). High-efficiency broadband anti-Stokes emission from Yb^{3+} -doped bulk crystals. *Optics Letters* 41: 2141–2144. <https://doi.org/10.1364/ol.41.002141>.